DIELECTRIC, VISCOUS, AND ELASTIC PROPERTIES OF MESOGENIC 4-*n*-HEXYLOXY-4′-CYANOBIPHENYL

G. Czechowski and J. Jadżyn

Institute of Molecular Physics, Polish Academy of Sciences
Smoluchowskiego 17, 60-179 Poznań, Poland

(Received January 22, 2001)

The paper presents the results of measurements of the static and dynamic electric permittivity, the shear viscosity, and the splay and bend elastic constants for 4-*n*-hexyloxy-4′-cyanobiphenyl ($C_6H_{13}O$–Ph–Ph–C≡N). On the basis of the static values of the nematic principal permittivities, $\varepsilon_{\parallel}(T)$ and $\varepsilon_{\perp}(T)$, the angle between the dipole moment vector and the long axis of 4-*n*-hexyloxy-4′-cyanobiphenyl molecule, the apparent dipole moment and the nematic order parameter were determined. From the temperature dependences of the dielectric relaxation time (corresponding to the molecular rotation around the short axis) and the shear viscosity, the strength of the nematic potential and the effective length of 4-*n*-hexyloxy-4′-cyanobiphenyl molecule (in isotropic phase) were estimated. The K_{11} and K_{33} elastic constants were determined from the voltage dependence of the capacitance of the planar nematic cell with the method proposed by Gruler et al. and Uchida et al.

PACS numbers: 64.70.Md, 77.84.Nh, 77.22.Gm, 66.20.+d

1. Introduction

A combination of anisotropic properties and fluidity of the nematic liquid crystals makes these materials unusual from both the basic research and the technical points of view. The most important result of the combination is a possibility of control of the molecular orientation in the whole nematic sample with an external electric or magnetic field of a relatively low strength. This circumstance is important from the molecular physics point of view, as allows to study the macroscopic properties of nematic liquid crystals in relation to the direction of the principal axes of the nematogenic molecules [1–4]. In case of the static dielectric studies, the temperature dependence of the principal permittivities, $\varepsilon_{\parallel}(T)$ and $\varepsilon_{\perp}(T)$, leads to such important molecular quantity as the angle between the dipole moment of the

mesogenic molecule and its long axis [5, 6]. It is a unique experimental method yielding this quantity in the liquid state.

The frequency dependence of the nematic complex electric permittivity allows to study the dynamics of mesogenic molecules. The rod-like shape of the molecules makes the interpretation of the dielectric relaxation spectra $\varepsilon^*_{\parallel}(\omega)$ and $\varepsilon^*_{\perp}(\omega)$ quite perspicuous as the molecular rotations around the three axes of symmetry (the long and short molecular axes and the director $\boldsymbol{n}$) manifest themselves in the spectra as quite well separated absorption bands. There is no doubt that the analysis of the absorption band corresponding to the molecular rotation around the short axis is the most informative since together with the viscosity data, the strength of the nematic potential and the effective length of the rotating molecule (in the isotropic phase) can be estimated.

Numerous applications of the nematic liquid crystals result from peculiar elastic properties of these materials. Determination of the elastic constants is based on the measurements of distortion of the director $\boldsymbol{n}$ caused by an external electric or magnetic field. In principle, the elastic constants corresponding to the three basic distortions of the nematic liquid crystals: splay (K_{11}), twist (K_{22}), and bend (K_{33}) can be obtained from three experiments. In two of them, the electric field induces the director distortion in planar (K_{11}) or twisted planar (K_{22}) cell and in the third experiment a magnetic field causes the distortion in the homeotropic cell (K_{33}). In case of a strong anchoring of the nematic molecules at the cell surfaces, the distortions have a threshold character (Freedericksz transition). Then, the elastic constants K_{ii} $(i = 1, 2, 3)$ can be calculated on the basis of the threshold value of the voltage (U_{th}) or magnetic field (B_{th}), respectively, provided the dielectric or magnetic anisotropy of the studied liquid crystal is known.

The most studies on the elasticity of the nematics concern the splay and bend constants only, since these constants essentially govern such switching characteristics as the threshold voltage or the response time. Many experimental methods were elaborated for determination of K_{11} and K_{33} elastic constants. The most widespread are based on the optical or capacitive observations of the director distortion in a pre-oriented nematic cell [7–11]. In this paper the elastic constants K_{11} and K_{33} were determined with the capacitance method.

2. Experimental

4-*n*-hexyloxy-4′-cyanobiphenyl ($C_6H_{13}O$–Ph–Ph–C≡N, 6OCB) was synthesized and purified at the Institute of Chemistry, Military University of Technology, Warsaw. The compound has the following sequence of the phase transitions: crystal (Cr) 58°C – nematic (N) 76°C – isotropic (I).

The static electric permittivity and conductivity were measured with a Wayne Kerr 6425 Precision Component Analyser at the frequency of 10 kHz. The nematic sample, placed between two plane electrodes of the capacitor, was oriented with a magnetic field of about 0.6 T. The components of permittivity ($\varepsilon_{\parallel}$ and $\varepsilon_{\perp}$) and conductivity ($\sigma_{\parallel}$ and $\sigma_{\perp}$) were simultaneously measured for appropriate orientation of the measuring electric field $\boldsymbol{E}$ with respect to the orienting magnetic field $\boldsymbol{B}$: $\boldsymbol{E} \parallel \boldsymbol{B}$ and $\boldsymbol{E} \perp \boldsymbol{B}$, respectively.

The dielectric relaxation spectra were recorded with a HP 4194A Impedance/ Gain-Phase Analyser in the frequency range of 100 kHz–100 MHz. The measuring capacitor consisted of three plane electrodes: one central ("hot") electrode and two grounded electrodes on each side. The external biasing d.c. electric field was used for ordering the nematic sample. Of course, in such circumstances only the dielectric spectrum $\varepsilon^*_{\parallel}(\omega)$ can be recorded.

The density was measured with an Anton Paar DMA 60/602 vibration tube densimeter.

The viscosity was measured with a Haake viscometer Rotovisco RV20 with the measuring system CV 100. The system consists of the rotary beaker filled with the substance being studied and the cylindrical sensor of the Mooney–Evart type (ME15), placed in the center of the beaker. The liquid gap was 0.5 mm.

For the elastic constants measurements, the nematic 6OCB was placed in the LINKAM cell consisting of two flat ITO coated glass plates with a spacing of 5 μm. Due to the brushed polyimide treatment of the electrode surfaces, the nematic molecules were oriented planar with respect to the electrodes. The probe sinusoidal voltage of the HP 4284A Precision LCR-meter up to 20 V_{rms}, at 1 kHz, was applied and the cell capacitance as a function of the applied voltage was recorded. The voltage step was 20 mV in the vicinity of the Freedericksz transition and 200 mV for the higher voltage.

3. Results and discussion

3.1. Static permittivities

The temperature dependences of the static permittivities measured for the nematic and isotropic phases of 6OCB are presented in Fig. 1a. The results can be interpreted with the use of the Maier–Meier theory [12], according to which the permittivities measured, respectively, parallel ($\varepsilon_{\parallel}$) and perpendicular ($\varepsilon_{\perp}$) to the director $\boldsymbol{n}$, are related to the molecular quantities by the following equations:

$$\varepsilon_{\parallel}(T) = 1 + \frac{NhF}{\varepsilon_0}\left\{\overline{\alpha} + \frac{2}{3}\Delta\alpha S + F\frac{\mu^2_{\mathrm{app}}}{3kT}\left[1 - (1 - 3\cos^2\beta)S\right]\right\}, \tag{1}$$

$$\varepsilon_{\perp}(T) = 1 + \frac{NhF}{\varepsilon_0}\left\{\overline{\alpha} - \frac{1}{3}\Delta\alpha S + F\frac{\mu^2_{\mathrm{app}}}{3kT}\left[1 + \frac{1}{2}(1 - 3\cos^2\beta)S\right]\right\}, \tag{2}$$

where $\varepsilon_0 = 8.85 \times 10^{-12}$ F $\cdot$ m^{-1}, h and F are the Onsager local field factors [13]. N is the number of molecules per unit volume calculated from the measured density of 6OCB (Fig. 2).

In the Maier–Meier theory the mesogenic molecules are considered as spherical, however their polarizability is anisotropic. In Eqs. (1) and (2) the $\overline{\alpha}$ and $\overline{\varepsilon}$ are the mean values of the polarizability and the permittivity, respectively

$$\overline{\alpha} = \frac{1}{3}(\alpha_l + 2\alpha_t), \qquad \overline{\varepsilon} = \frac{1}{3}(\varepsilon_{\parallel} + 2\varepsilon_{\perp}), \tag{3}$$

and

$$\Delta\alpha = \alpha_l - \alpha_t \tag{4}$$

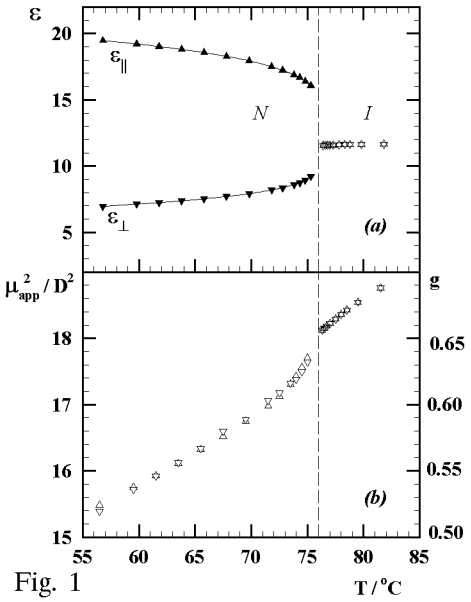

Fig. 1

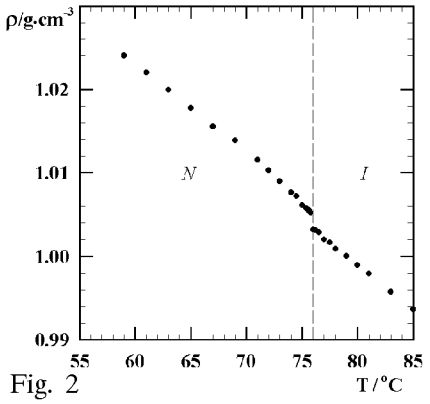

Fig. 2

Fig. 1. The solid lines in (a) are the best fitting of the Maier–Meier Eqs. (1) and (2) to the experimental values of static permittivities (points) of 6OCB for $\beta = 17°$ and $z = 0.208$. $\mu^2_{\rm app}(T)$ resulting from the fitting is presented in (b).

Fig. 2. Temperature dependence of the density of 6OCB in the isotropic and nematic phases.

denotes the anisotropy of polarizability. The α_l and α_t are respectively, the longitudinal and transversal components of the molecular polarizability. β in Eqs. (1) and (2) is the angle between the total dipole moment vector μ of the nematogenic molecule and its long axis and S is the order parameter defined as

$$S = \frac{1}{2}\langle 3\cos^2\Theta - 1\rangle, \tag{5}$$

where Θ is the angle between the long molecular axis and the director $\boldsymbol{n}$.

For isotropic phase ($\varepsilon_\parallel = \varepsilon_\perp = \varepsilon$, $S = 0$), Eqs. (1) and (2) transform into Onsager equation [13]:

$$\frac{(\varepsilon - \varepsilon_\infty)(2\varepsilon + \varepsilon_\infty)}{\varepsilon(\varepsilon_\infty + 2)^2} = \frac{N}{3\varepsilon_0}\frac{\mu^2_{\rm app}}{3kT}, \tag{6}$$

where ε_∞ denotes the high frequency value of the permittivity (often taken as the refraction index square n^2).

There are three unknown quantities in Eqs. (1) and (2). Two of them concern the nematogen molecule and they are: (i) the angle β between the resultant dipole moment μ of the molecule and its long axis and (ii) the square of the apparent dipole moment $\mu^2_{\rm app}$ of the molecule; the third one is the macroscopic order parameter $S(T)$. These three quantities can be obtained from the fitting of the Maier–Meier equations to the experimental data [5]. The fitting procedure

becomes quite effective when the $S(T)$ dependence is expressed in an empirical formula [14]:

$$S(T) = \left(1 - \frac{T}{T_{\mathrm{NI}}}\right)^{z}, \tag{7}$$

where T_{NI} denotes the nematic to isotropic phase transition temperature. The temperature dependence of the nematic order parameter is then determined by one parameter (z) only.

The values of $\overline{\alpha} = 35.20 \times 10^{-24}$ cm^3 and $\Delta\alpha = 23.25 \times 10^{-24}$ cm^3 for 6OCB were taken from [15].

The solid lines in Fig. 1a represent the best fitting of Eqs. (1) and (2) to the measured permittivities. The postulated in [5] requirement of the equality of $\mu^2_{\mathrm{app}}(T)$ resulting from $\varepsilon_{\parallel}(T)$ and $\varepsilon_{\perp}(T)$ dependences is fulfilled, as shows Fig. 1b. The fitting leads to the following values of the parameters: $\beta = 17°$ and $z = 0.208$. The value obtained for β is expected and corresponds to β obtained for other nematogenic molecules of similar structure [5, 16] and is close to β value resulting from the quantum-chemical calculations (19°).

The solid line in Fig. 3 represents the $S(T)$ function plotted for $z = 0.208$ (Eq. (7)). The $S(T)$ dependence obtained is quite close to that resulting from the optical studies [15, 17].

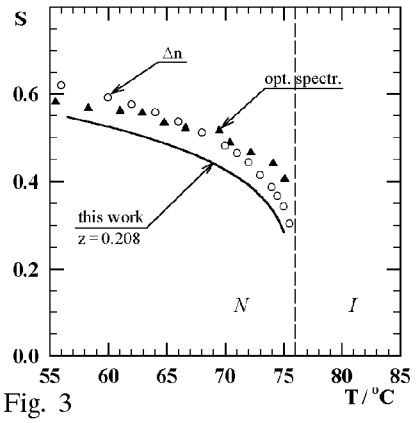

Fig. 3

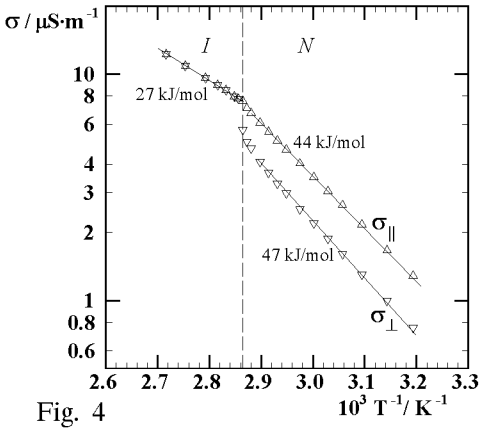

Fig. 4

Fig. 3. Order parameter of nematic 6OCB obtained from the static permittivities and from Δn [15] and spectroscopic [17] measurements.

Fig. 4. Arrhenius plots for the conductivity measured in isotropic and nematic phases of 6OCB. The values of the activation energy are given in the picture.

In Fig. 1b the values of the $\mu^2_{\mathrm{app}}(T)$ are expressed in the dimensionless Kirkwood correlation factor $g = \mu^2_{\mathrm{app}}/\mu^2_0$, with the dipole moment of a single 6OCB molecule μ_0 equal to 5.0 D [18]. The g-values smaller than the unity indicate the antiparallel dipolar correlations. Figure 1b shows that the transition from the isotropic phase to the nematic phase of 6OCB manifests itself by an essential increase in degree of the antiparallel dipolar association.

Figure 4 presents the temperature dependence of the ionic conductivity of 6OCB in the isotropic and nematic phases. As usual for the nematic liquid crystals, the conductivity in the direction of macroscopic molecular ordering ($\sigma_{\parallel}$) is higher than in the perpendicular direction ($\sigma_{\perp}$) with the activation energy somewhat higher for $\sigma_{\perp}$. In the isotropic phase of 6OCB the conductivity activation energy is essentially smaller as compared with that in the nematic phase.

3.2. Dielectric relaxation

Figure 5 presents the dielectric relaxation spectra recorded in the isotropic and nematic phases of 6OCB. In the latter phase the permittivity was measured for $\boldsymbol{E} \parallel \boldsymbol{n}$. The analysis of the dielectric relaxation spectra of 6OCB can be carried

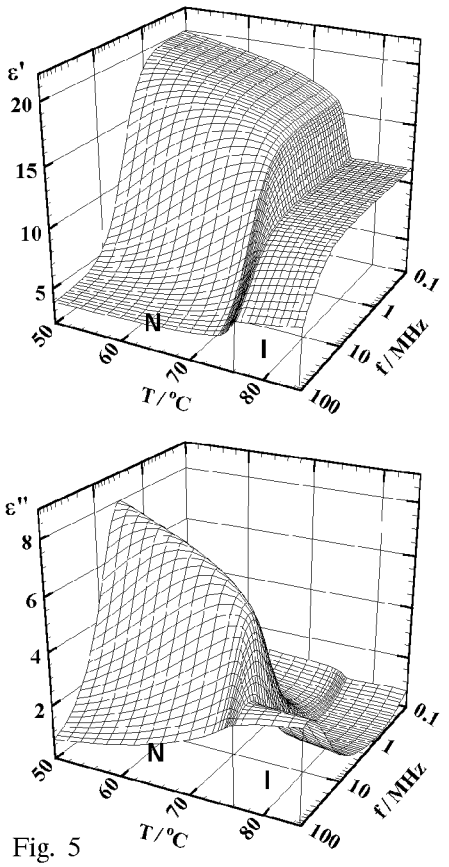

Fig. 5

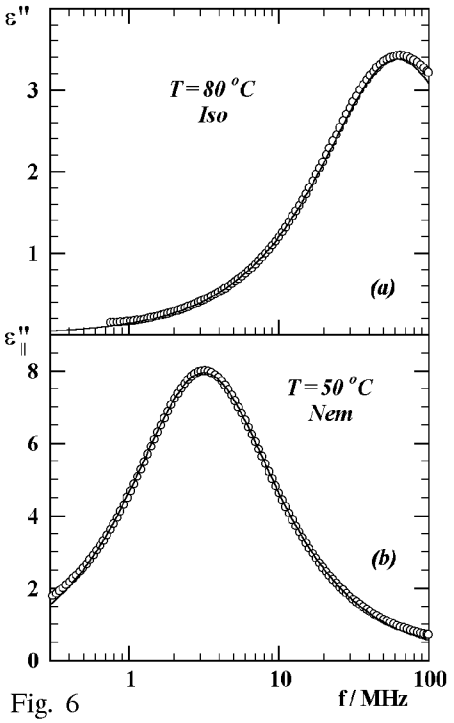

Fig. 6

Fig. 5. Frequency and temperature dependence of the real (ε') and the imaginary (ε'') parts of the electric permittivity of 6OCB in the isotropic and nematic phases. In nematic phase the permittivity $\varepsilon^*_{\parallel}(\omega, T)$ was measured.

Fig. 6. An example of the dielectric absorption spectrum recorded in the (a) isotropic and (b) nematic phases of 6OCB. Solid lines correspond to the Debye-type curves.

out in the framework of the molecular model presented in [19]. According to the model, in oriented nematic sample, the nematogen molecule rotates around the three axes of symmetry: two of them concern the molecule itself (the long and short molecular axes) and the third axis is the director $\boldsymbol{n}$. For a typical nematogen substances (like 6OCB), the electromagnetic energy absorption due to these three modes of rotation can be expected in the frequency region from several megahertz to several gigahertz [20, 21].

As shows Fig. 6, in the studied frequency range one dielectric absorption band strongly dominates both in the isotropic and nematic phases of 6OCB. The band corresponds to the molecular rotation around the short axis and, as seen in Fig. 6, can be perfectly described with the simple Debye formula

$$\varepsilon^*(\omega) = \varepsilon'(\omega) - \mathrm{j}\varepsilon''(\omega) = \varepsilon_\infty + \frac{A}{1 + \mathrm{j}\omega\tau}, \tag{8}$$

where A and τ denote the dielectric strength and the relaxation time, respectively.

The temperature dependences of the dielectric strength A and the relaxation time τ are presented in Fig. 7. At the temperature of the phase transition from the isotropic to nematic phase one observes a strong increase in the values of A

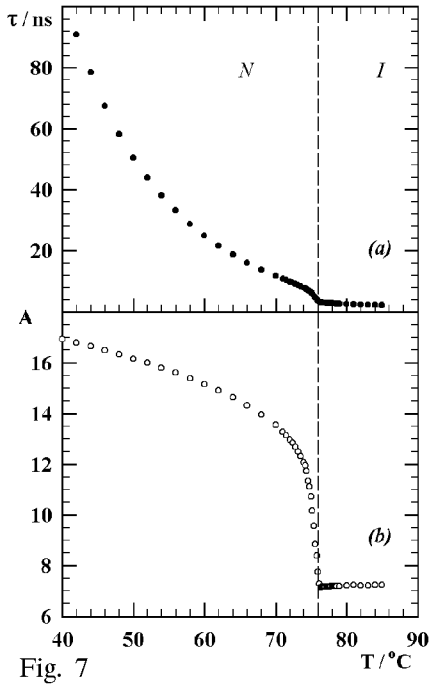

Fig. 7

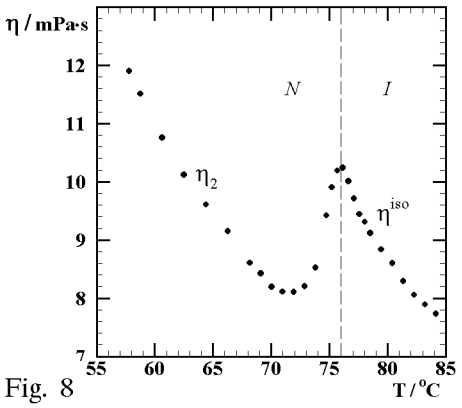

Fig. 8

Fig. 7. Temperature dependence of the relaxation time (a) and the dielectric strength (b) corresponding to 6OCB molecular rotation around the short axis.

Fig. 8. Temperature dependence of the shear viscosity of the freely flowing 6OCB in isotropic and nematic phases.

and τ. The temperature dependence of the relaxation time τ can be interpreted if the viscosity of the medium is known.

Figure 8 shows the temperature dependence of the viscosity of 6OCB measured in the isotropic and nematic phases. At the isotropic to nematic transition temperature a sharp decrease in the viscosity is observed. It is due to the flow alignment effect occurring in the nematic phase [1]. The effect leads to the situation where the macroscopic ordering of the flowing nematic liquid crystal becomes (roughly) parallel to the velocity v and perpendicular to the velocity gradient. Then, the nematic viscosity has the least possible value. In terms of the Mięsowicz viscosity coefficients [22], the viscosity measured in our experiment is close to η_2.

Figure 9 presents the Arrhenius plots for the dielectric relaxation time and the viscosity in the isotropic and nematic phases of 6OCB. In the isotropic phase the activation energy for the molecular rotation around the short axis and that of the viscous flow, are quite close to each other. It means that the viscosity is the main factor, which determines the molecular dynamics in the isotropic phase of 6OCB. If so, one can use the Debye model [23] for evaluation of the effective length of the 6OCB molecule. In the model, the rotating dipolar, rigid, and axially symmetric molecule is represented by the sphere of a diameter ℓ. The relation between the dielectric relaxation time, corresponding to the molecular rotation around its short axis (τ) and the viscosity (η) of the isotropic medium in which the sphere is moving, has the following form:

$$\tau^{\mathrm{iso}} = \frac{\pi \ell^3 \eta^{\mathrm{iso}}}{2kT}, \tag{9}$$

where T is the absolute temperature, and k — the Boltzmann constant. The linear dependence of the relaxation time to viscosity ratio on T^{-1}, predicted by this very simplified model, is quite well fulfilled here (Fig. 10). The slope of the dependence gives a reasonable value $\ell \approx 17$ Å for the length of 6OCB molecule.

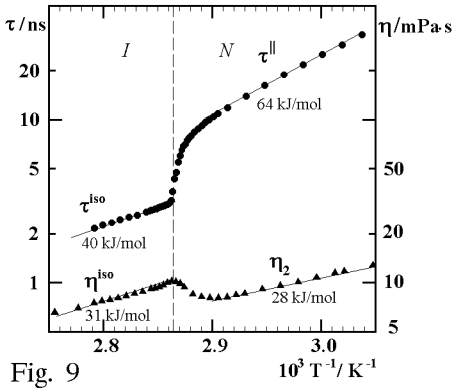

Fig. 9

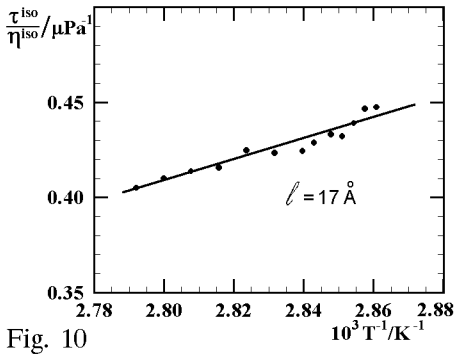

Fig. 10

Fig. 9. Arrhenius plots for the relaxation time corresponding to the molecular rotation around the short axis and for the shear viscosity of the freely flowing 6OCB. The values of the activation energy are given in the figure.

Fig. 10. Debye plot (Eq. (9)) for 6OCB in the isotropic phase.

The quantum-chemical estimation leads to quite close value $\ell \approx 19$ Å. Figure 9 shows that the value of the viscosity activation energy is practically the same in the isotropic and nematic phases of 6OCB. In case of the dielectric relaxation time, the transition to the nematic phase manifests itself by a strong increase in the activation energy for the molecular rotation around the short axis. On the basis of these two experimental data the strength of the nematic potential can be estimated as a difference between the activation energy for the molecular reorientation and that for the viscosity of the medium [4].

3.3. Elastic constants

The capacitance method of determination of splay (K_{11}) and bend (K_{33}) elastic constants consists in the analysis of the voltage dependence of the capacity of the planar nematic cell. In case of nematic liquid crystals with a positive dielectric anisotropy ($\Delta\varepsilon = \varepsilon_{\parallel} - \varepsilon_{\perp} > 0$), the probing electric field $\boldsymbol{E}$ of a sufficient intensity causes a distortion of the director (Fig. 11). With the increase in the field intensity, the capacity of the cell increases from the initial value $C_{\perp}$ — corresponding to $\boldsymbol{n} \perp \boldsymbol{E}$, to the final value $C_{\parallel}$ — corresponding to $\boldsymbol{n} \parallel \boldsymbol{E}$ (Figs. 12 and 13). The phenomenon has the threshold, i.e. the capacity is on the voltage dependent when the voltage reaches characteristic of a given nematic liquid crystal value U_{th}. This value is the basic quantity for calculation of the splay elastic constant

$$K_{11} = \varepsilon_0 \Delta\varepsilon U_{\mathrm{th}}^2/\pi^2, \tag{10}$$

where $\varepsilon_0 = 8.85$ pF/m. Figure 12 shows an example of Freedericksz transition in planar 6OCB nematic cell at 60°C.

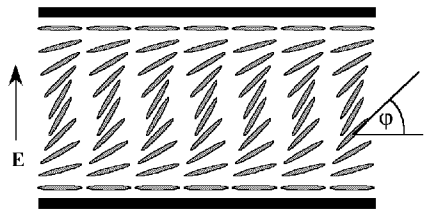

Fig. 11

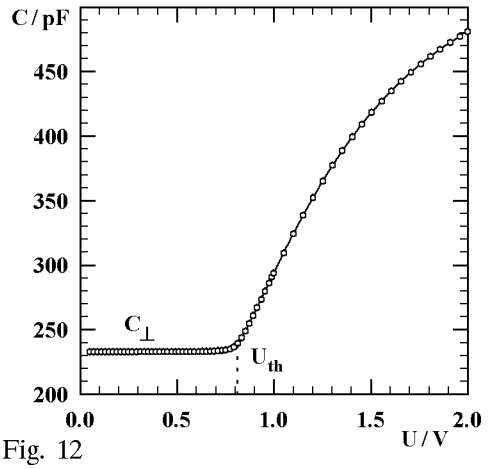

Fig. 12

Fig. 11. Distortion of the director $\boldsymbol{n}$ in the planar nematic cell caused by the voltage higher than the Freedericksz threshold value U_{th}.

Fig. 12. Voltage dependence of the capacity of planar 6OCB nematic cell in the vicinity of threshold voltage U_{th} for Freedericksz transition at 60°C.

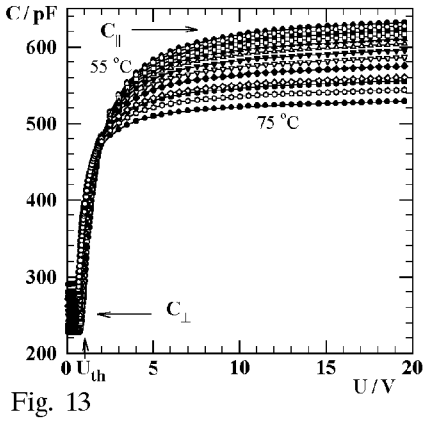

Fig. 13

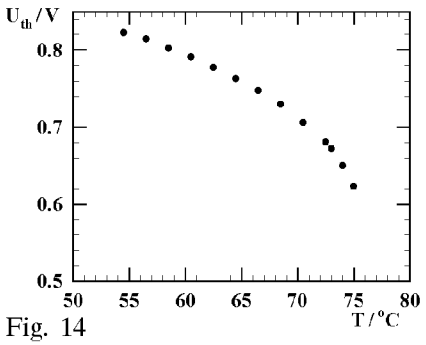

Fig. 14

Fig. 13. C vs. U in the whole range of the applied voltage at different temperatures (step 2°C).

Fig. 14. Temperature dependence of the threshold voltage for Freedericksz transition in the planar 6OCB nematic cell.

Figure 14 presents the temperature dependence of the voltage threshold value $U_{\rm th}$ for the Freedericksz transition in 6OCB planar cell and Fig. 15 shows the dependence for the splay elastic constant K_{11} calculated from Eq. (10). The values of the dielectric anisotropy $\Delta\varepsilon$ of 6OCB were calculated from the data presented in Fig. 1a. As seen in Fig. 15, the values obtained for K_{11} elastic constant agree very well with the results of Bradshaw et al. [24].

The K_{33} elastic constant can be determined in the same experiment from the analysis of the dependence of the cell capacitance on the voltage *above the threshold value*. The exact equation describing the $C(U)$ dependence was obtained first by Gruler et al. [25]. Next, Uchida and Takahashi [26] proposed a procedure for the K_{33} determination, which eliminates the need of a multiparameter least squares fitting of Gruler et al. equation to the experimental data. The final equation for $C(U)$ dependence has the following form [27, 28]:

$$\frac{C(U)-C_{\perp}}{C_{\perp}} = \gamma - \frac{2\gamma}{\pi}\frac{U_{\rm th}}{U}\left(1+\gamma\sin^2\varphi_m\right)^{1/2} \times \int_0^{\varphi_m}\left[\frac{(1+\chi\sin^2\varphi)(1-\sin^2\varphi)}{(1+\gamma\sin^2\varphi)(\sin^2\varphi_m-\sin^2\varphi)}\right]^{1/2}\cos\varphi{\rm d}\varphi, \tag{11}$$

where $\chi = K_{33}/K_{11}-1$, $\gamma = \varepsilon_{\parallel}/\varepsilon_{\perp}-1$, ϕ is the tilt angle between the director $\boldsymbol{n}$ and the cell walls and φ_m is the tilt angle at the center of the cell.

For the voltage much higher than the threshold value, the director $\boldsymbol{n}$ at the center of the cell becomes perpendicular to the cell walls and $\varphi_m = \pi/2$. Then, Eq. (11) reduces to

$$\frac{C(U)-C_{\perp}}{C_{\perp}} = \gamma - \frac{2\gamma}{\pi}\frac{U_{\rm th}}{U}(1+\gamma)^{1/2}\int_0^{\pi/2}\left(\frac{1+\chi\sin^2\varphi}{1+\gamma\sin^2\varphi}\right)^{1/2}\cos\varphi{\rm d}\varphi. \tag{12}$$

This equation predicts that for $U \gg U_{\rm th}$ the dependence $(C - C_\perp)/C_\perp$ on U^{-1} should be linear. The extrapolation of the dependence to $U^{-1} = 0$ leads directly to the value of $\gamma = \Delta\varepsilon/\varepsilon_\perp$ and the slope

$$\alpha = \frac{2\gamma}{\pi}(1+\gamma)^{1/2} U_{\rm th} \int_0^{\pi/2} \left(\frac{1+\chi\sin^2\varphi}{1+\gamma\sin^2\varphi}\right)^{1/2} \cos\varphi \mathrm{d}\varphi \tag{13}$$

contains only one unknown quantity $\chi = K_{33}/K_{11} - 1$. Therefore, the K_{33} constant can be easily obtained since the K_{11} constant is known from Eq. (10).

The results of measurements of the $C(U)$ dependence for planar 6OCB nematic cell in the whole range of the applied voltage are depicted in Fig. 13. In the used range of voltage, the capacity of the cell changes from $C_\perp$ (for $U < U_{\rm th}$) to close to $C_\parallel$ (for $U \gg U_{\rm th}$).

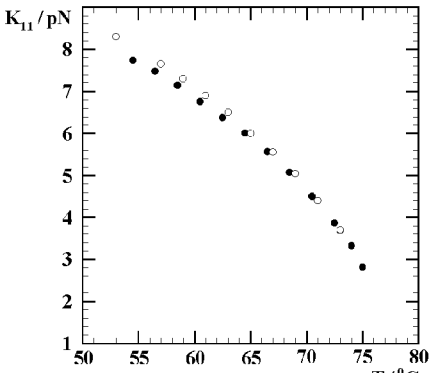

Fig. 15

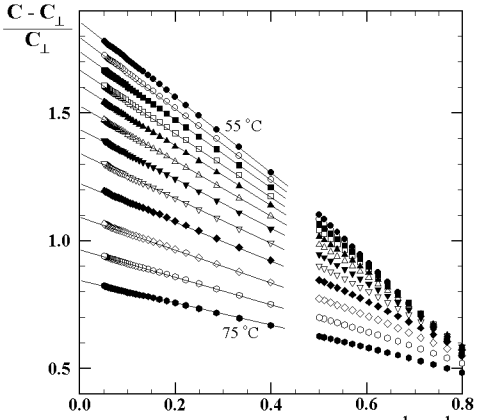

Fig. 16

Fig. 15. Temperature dependence of the splay elastic constant of 6OCB. The open points are the results of Bradshaw et al. [24].

Fig. 16. $(C - C_\perp)/C_\perp$ on U^{-1} dependences for nematic 6OCB at different temperatures (step 2°C).

According to Eq. (12), the theory predicts that for the voltages much higher than $U_{\rm th}$, the change of the cell capacity should be proportional to the reciprocal of U. The results presented in Fig. 16 show that this prediction is well fulfilled: for U higher than about 4 V the dependences $C(U^{-1})$ are linear. The extrapolation of these linear dependences to $U^{-1} = 0$, leads to the value of $(C_\parallel - C_\perp)/C_\perp$, i.e. to $(\varepsilon_\parallel - \varepsilon_\perp)/\varepsilon_\perp$, the quantity which can be directly determined in the static dielectric measurements of the nematic sample oriented with a magnetic field, for example. In Fig. 17 the values of $(\varepsilon_\parallel - \varepsilon_\perp)/\varepsilon_\perp$ obtained for 6OCB from the extrapolation procedure are compared with those obtained in direct static dielectric measurements presented in Fig. 1a. Perfect agreement of these two results is a good test for consistency of the experimental procedure and the theory.

As was mentioned above, the slope α of the $(C - C_\perp)/C_\perp$ on U^{-1} linear dependence, as shows Eq. (13), leads to the value of $\chi = K_{33}/K_{11} - 1$ and hence to the K_{33} elastic constant, because the K_{11} constant is known.

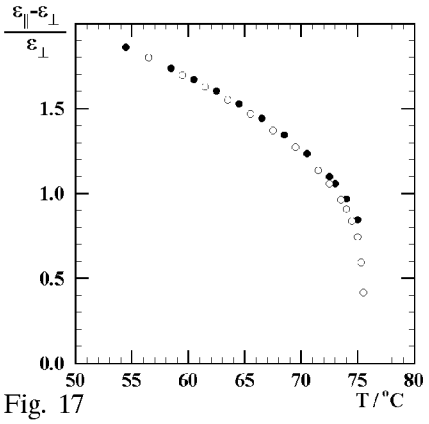

Fig. 17

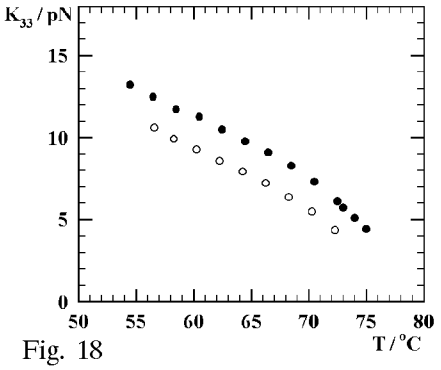

Fig. 18

Fig. 17. Temperature dependence of $(\varepsilon_{\parallel} - \varepsilon_{\perp})/\varepsilon_{\perp}$ for 6OCB determined from the extrapolation of $(C - C_{\perp})/C_{\perp}$ to $U^{-1} = 0$ (Eq. (12)) (full points) and measured in the sample oriented with magnetic field (open points are the results from Fig. 1a).
Fig. 18. Temperature dependence of the bend elastic constant of 6OCB calculated with Eq. (13) (full points) and the results of Bradshaw (open points) [24].

Figure 18 presents the temperature dependence of the bend elastic constant of 6OCB obtained with the capacitance method. The results are quite close to that obtained by Bradshaw et al. [24] with the use of the cell with the homeotropic molecular ordering and the magnetic field as an external force for the director $\boldsymbol{n}$ distortion. The results presented in this paper show that the reliable data for K_{33} elastic constant can be obtained with the simple capacitance method in the same experiment in which the K_{11} constant is determined from the Freedericksz transition in planar nematic cell.

Acknowledgment

The work was partially supported by the Polish Research Project No. 2PO3B 032 18 coordinated by the Committee for Scientific Research.

References

[1] P.G. de Gennes, J. Prost, *The Physics of Liquid Crystals*, 2nd edition, Clarendon Press, Oxford 1993.

[2] W.D. de Jeu, *Physical Properties of Liquid Crystalline Materials*, Ed. G.W. Gray, Gordon and Breach Sci. Publ., New York 1980.

[3] D. Dunmur, K. Toriyama, *Physical Properties of Liquid Crystals*, Eds. D. Demus, J. Goodby, G.W. Gray, H.-W. Spiess, V. Vill, Wiley-VCH, Weinheim 1999, p. 129.

[4] G. Williams, *The Molecular Dynamics of Liquid Crystals*, Eds. G.R. Luckhurst, C.A. Veracini, Kluwer Academic Press, Dordrecht 1994, p. 431.

[5] J. Jadżyn, S. Czerkas, G. Czechowski, A. Burczyk, *Liq. Cryst.* **26,** 437 (1999).

[6] S. Urban, J. Kędzierski, R. Dąbrowski, *Z. Naturforsch. A* **55,** 449 (2000).

[7] H. Schad, G. Baur, G. Meier, *Appl. Phys.* **17,** 177 (1978).

[8] H.J. Deuling, *Solid State Physics, Suppl.* **14,** 77 (1978).

[9] M. Schadt, P.R. Gerber, *Z. Naturforsch. A* **37,** 165 (1982).

[10] P.R. Gerber, M. Schadt, *Z. Naturforsch. A* **35,** 1036 (1980).

[11] R. Barberi, G. Barbero, M. Moldovan, *Phys. Rev. E* **50,** 1093 (1994).

[12] W. Maier, G. Meier, *Z. Naturforsch. A* **16,** 262 (1961).

[13] L. Onsager, *J. Am. Chem. Soc.* **58,** 1486 (1936).

[14] A. Buka, W.H. de Jeu, *J. Phys. (Paris)* **43,** 361 (1982).

[15] M. Mitra, *Mol. Cryst. Liq. Cryst.* **241,** 17 (1994).

[16] A. Ferrarini, P.L. Nordio, *Mol. Cryst. Liq. Cryst.* **198,** 159 (1991).

[17] H. Moryson, H. Kozłowski, D. Bauman, *Mol. Cryst. Liq. Cryst.* **331,** 2299 (1999).

[18] C. Druon, Ph.D. thesis, University of Lille, 1984.

[19] J. Jadżyn, G. Czechowski, R. Douali, C. Legrand, *Liq. Cryst.* **26,** 1591 (1999).

[20] S. Urban, B. Gestblom, H. Kresse, R. Dąbrowski, *Z. Naturforsch. A* **51,** 834 (1996).

[21] S. Urban, *Z. Naturforsch. A* **54,** 305 (1999).

[22] M. Mięsowicz, *Nature* **136,** 261 (1935); **158,** 27 (1946).

[23] C.J.F. Böttcher, P. Bordewijk, *Theory of Electric Polarization*, Vol. II, Elsevier Sci., Amsterdam 1978.

[24] M.J. Bradshaw, E.P. Raynes, J.D. Bunning, T.E. Faber, *J. Phys. (Paris)* **46,** 1513 (1985).

[25] H. Gruler, T.J. Scheffer, G. Meier, *Z. Naturforsch. A* **27,** 966 (1972).

[26] T. Uchida, Y. Takahashi, *Mol. Cryst. Liq. Cryst.* **72,** 133 (1981).

[27] P. Chattopadhayay, S.K. Roy, *Mol. Cryst. Liq. Cryst.* **257,** 89 (1994).

[28] Y. Zhou, S. Sato, *Jpn. J. Appl. Phys.* **36,** 4397 (1997).